Plasma Sources Science and Technology

PAPER

Three-electrode surface dielectric barrier discharge driven by repetitive pulses: streamer dynamic evolution and discharge mode transition

To cite this article: Bangfa Peng *et al* 2024 *Plasma Sources Sci. Technol.* **33** 045018

IOP Publishing Plasma Sources Science and Technology

Plasma Sources Sci. Technol. 33 (2024) 045018 (15pp) https://doi.org/10.1088/1361-6595/ad3a9e

Three-electrode surface dielectric barrier discharge driven by repetitive pulses: streamer dynamic evolution and discharge mode transition

Bangfa Peng[1,*], Nan Jiang[2,*], Yifei Zhu[3], Jie Li[2] and Yan Wu[2]

[1] Shanxi Key Laboratory of Mining Electrical Equipment and Intelligent Control, College of Electrical and Power Engineering, Taiyuan University of Technology, Taiyuan 030024, People's Republic of China
[2] School of Electrical Engineering, Dalian University of Technology, Dalian 116024, People's Republic of China
[3] School of Electrical Engineering, Xi'an Jiaotong University, Xi'an 710049, People's Republic of China

E-mail: pengbangfa@tyut.edu.cn and jiangnan@dlut.edu.cn

Received 27 July 2022, revised 23 February 2024
Accepted for publication 4 April 2024
Published 29 April 2024

Abstract

The streamer dynamic evolution and discharge mode transition of a three-electrode surface dielectric barrier discharge (SDBD) driven by repetitive pulses are studied experimentally and numerically for better plasma-mode control and optimized application. Spatial-temporal plasma morphologic features together with electro-optical behavior are utilized to analyze the streamer dynamic evolution and streamer-to-spark transition. To gain a deep insight into the physical mechanism of the discharge mode transition in repetitive pulses, a 2D fluid model combined with a 0D kinetic model is built and studied. A good agreement between the experimental measurements and numerical simulation in the propagation dynamics and voltage–current characteristics is achieved. The results show that the surface-streamer discharge in the form of primary and transitional streamers can transform into a surface-spark discharge characterized by the primary streamer, transitional streamer and spark phase in repetitive pulses under the high applied electric field. A high gas temperature will result in a large reduced electric field after the transitional streamer, which exceeds the ionization threshold and thus promotes the discharge mode transition. A high number of electrons can be released from the negative charges by oxygen atoms during the inter-pulse period, which is favorable for the re-ignition and ionization process of the subsequent pulse discharge.

Keywords: discharge mode transition, streamer dynamic evolution, surface-streamer, surface-spark, repetitive pulses, three-electrode SDBD

1. Introduction

Pulsed discharge has attracted significant interest due to its prospective applications, including flow control [1], medical therapy [2], icing mitigation [3] and environmental remediation [4]. Generally, these different application fields will adopt different discharge modes based on their predominant plasma physical–chemical properties. For example, the streamer discharge is considered to be a suitable choice for pollutant degradation [5] and ozone generation [6] because of the low energy cost and high chemical activity. The spark discharge shows potential prospects in ice-breaking due to the shock wave and high-energy density [7]. Fortunately, the

[*] Authors to whom any correspondence should be addressed.

different discharge modes can be obtained in the same geometry by varied parameters, such as repetitive pulses.

A repetitively pulsed discharge can lead to the accumulation of active species and charged species in the plasma region. As a result, the discharge behavior can be affected by the memory effects of residual species [8–10]. The residual charges and active species produced by the previous pulse can induce a subsequent streamer that is ignited from the stopping point of the preceding discharge in the volume discharge [11]. Also, this subsequent streamer can follow the old path of the plasma channel and can exhibit faster propagation velocity with large pulse-to-pulse intervals [12]. Besides, a repetitively pulsed discharge can also provide varied discharge modes because of the residual species and heating accumulations [13]. Under the long-term repetitive pulses, a transformation from the intermittent-mode to the continuous mode is also observed due to the residual space charges [14]. The fact that discharge mode transitions among a corona discharge, glow discharge and spark discharge can be formed in a pin–pin configuration through a varied pulse repetition frequency has been studied [15]. However, when a dielectric is introduced to the discharge gap, the discharge mode transition should be different compared to the discharge in a pure gas medium. The dielectric can be polarized by the electric field [16], so that it influences the attraction and propagation of the generated streamer. Moreover, the residual charges accumulated on a dielectric surface show different properties, including the charge deposition, transfer and decay [17–20], which can influence the plasma streamer propagation, plasma distribution and discharge mode [21, 22].

In this study, a three-electrode pulsed surface dielectric barrier discharge (SDBD) is proposed to realize and analyze the streamer dynamic evolution and discharge mode transition during a repetitively pulsed discharge with a dielectric. This configuration is developed from the typical two-electrode SDBD, in which a new second grounded (SG) electrode is arranged on the same side of a high-voltage (HV) electrode, and shows potential application in areas such as ice-breaking [7] based on the rapid energy release. In our previous works [23, 24], our results also showed that the surface-streamer discharge and surface-spark discharge can be formed in the three-electrode configuration when a single-shot pulse is performed. Also, the different streamer phases, including primary, transitional and secondary reverse streamers, were analyzed in a single pulse. Furthermore, detailed descriptions of streamer dynamic evolution and discharge mode transition in a three-electrode configuration operated with repetitive pulses should be obtained, and they play a critical role in revealing the deep physical mechanism of plasma-mode control and the various plasma-based applications.

To gain more knowledge of the underlying physical mechanism in the evolution of streamer phases and acquire a detailed understanding of the transition from surface-streamer to surface-spark discharge, experiments are performed by focusing on the streamer evolution and discharge mode transition in the three-electrode SDBD under consecutive pulses. Numerical simulation is proposed to analyze the mechanism for the formation of the surface-spark discharge in the repetition pulses. The investigation is conducted using electrical characteristics, optical measurements and numerical simulation, which are utilized to propose the descriptions of the discharge phase evolution and breakdown mode transition during the repetitively pulsed surface discharge process.

2. Experimental and numerical methods

2.1. Experimental method

A brief schematic of the experimental set-up is described in figure 1(a). A repetitive HV pulse generated from the pulse power (HVP-20P, Xi'an Smart Maple Electronic Technology Co. Ltd, China) is applied on the HV electrode to induce the formation of surface plasma. A HV probe (Tektronix P6015A) and a current probe (Tektronix P6021A) linked with a digital oscilloscope (Tektronix DPO 3012) are utilized to monitor the waveforms of the applied pulse voltage and discharge current simultaneously. An intensified charge-coupled device (ICCD) camera (PI-MAX-3 equipped with a Canon 50 mm f/1.8 UV lens), synchronized with the applied HV pulse, is adopted to capture the spatial-temporal evolution of different plasma phases in the three-electrode pulsed SDBD under repetitive pulses. A photomultiplier tube (Sens-Tech Model P30A-05) is utilized to measure the optical emission intensity of the surface-streamer discharge driven by consecutive pulses in the whole discharge gap.

A detailed description of the three-electrode SDBD configuration is shown in figures 1(b) and (c). The three-electrode SDBD configuration consists of a HV electrode, a dielectric, a first grounded (FG) electrode and an SG electrode. The dielectric is made of Teflon with a thickness of 1 mm. The HV electrode and the SG electrode consist of aluminum foil with a length of 70 mm, a width of 10 mm and a thickness of 0.1 mm. These two electrodes are arranged on the same side of the dielectric surface with a corresponding distance (9 mm and 13 mm). The FG electrode is also made of aluminum foil, with a length of 70 mm and a thickness of 0.1 mm. Moreover, the width of the FG electrode is consistent with the discharge gap between the HV electrode and the SG electrode, which is 9 mm and 13 mm in our experiment.

2.2. Plasma fluid model

The fundamental physical mechanism of the streamer dynamic evolution, including the variations of the electric field and species density, is difficult to obtain via experimental measurements. As a result, the mechanism of the surface-streamer evolution and discharge mode transition in the three-electrode pulsed SDBD are investigated using the plasma fluid model in 2D PASSKEy (PArallel Streamer Solver with KinEtics) [25], which has been validated by a series of experimental results, including plasma process, voltage–current characteristics

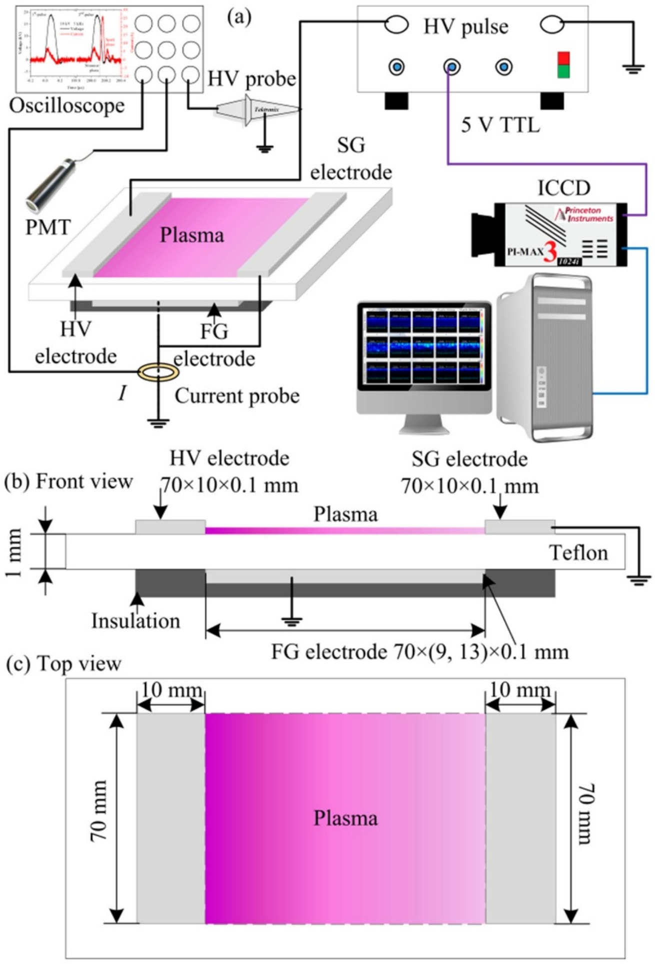

Figure 1. A brief description of the experimental set-up for three-electrode pulsed SDBD: (a) a diagram of the three-electrode pulsed SDBD; (b) the front view of three-electrode SDBD configuration; and (c) the top view of the three-electrode SDBD configuration.

and electric field evolutions from published studies [26, 27]. Detailed descriptions of the mathematical formulations, initial conditions and boundary conditions can be found in [27]. Here, a brief description of the 2D fluid model is shown in the following sections.

2.2.1. Governing formulations. The drift-diffusion-reaction equations for species, the electron energy equation for the mean electron energy and Poisson's equation for the electric field are shown as follows:

$$\frac{\partial n_i}{\partial t} + \nabla \cdot \boldsymbol{\Gamma}_i = S_i + S_{\mathrm{ph}}, \quad i = 1, 2, \ldots, N_{\mathrm{total}} \tag{1}$$

$$\boldsymbol{\Gamma}_i = \left(\frac{q_i}{|q_i|}\right) \mu_i n_i \boldsymbol{E} - D_i \nabla n_i, \quad i = 1, 2, \ldots, N_{\mathrm{charge}} \tag{2}$$

$$\frac{\partial}{\partial t}\left(n_{\mathrm{e}} \epsilon_{\mathrm{m}}\right) + \nabla \cdot \boldsymbol{\Gamma}_{\epsilon} = -|q_{\mathrm{e}}| \boldsymbol{\Gamma}_{\boldsymbol{e}} \cdot \boldsymbol{E} - P\left(\epsilon_{\mathrm{m}}\right) \tag{3}$$

$$\boldsymbol{\Gamma}_{\epsilon} = -\mu_{\epsilon} n_{\mathrm{e}} \epsilon_{\mathrm{m}} \boldsymbol{E} - D_{\epsilon} \nabla\left(n_{\mathrm{e}} \epsilon_{\mathrm{m}}\right) \tag{4}$$

$$\nabla\left(\varepsilon_0 \varepsilon_{\mathrm{r}} \nabla \Phi\right) = -\sum_{i=1}^{N_{\mathrm{charge}}} q_i n_i - \rho_{\mathrm{c}} \delta_{\mathrm{s}} \tag{5}$$

where n_i and $\boldsymbol{\Gamma}_i$ are the number density and species flux of species i, respectively; S_i and S_{ph} indicate the source of species generation and consumption from the selected 40 reactions with 18 species (see section of 2.2.2) and the photoionization sources, respectively; q_i, μ_i and D_i are the charge, mobility coefficient and diffusion coefficient of each species i, respectively; μ_{ϵ} and D_{ϵ} indicate the mobility coefficient and diffusion coefficient of the electron energy, respectively. And the corresponding rate coefficients of electron impact reactions are represented as explicit functions of the mean electron energy (ϵ_{m}) based on the local mean energy approximation (LMEA). The mobility coefficient and diffusion coefficient of ions come from [28]. For the neutral species, it is assumed that the $\nabla \cdot \boldsymbol{\Gamma}_{\boldsymbol{i}} = 0$ during the computational process due to the short time. Moreover, the neutral species are not affected by the electric field. Here, Φ and $P\left(\epsilon_{\mathrm{m}}\right)$ are the electric potential and the power lost by the electrons in collisions, respectively; $\boldsymbol{E}$ is the electric field with the expression $\boldsymbol{E} = -\nabla \Phi$; n_{e}, $\boldsymbol{\Gamma}_{\epsilon}$ and q_{e} are the electron density, electron energy flux and electron charge, respectively; ε_0, ε_{r}, ρ_{c} and δ_{s} indicate the vacuum permittivity, relative permittivity, charge density on the dielectric surface and Kronecker delta function (equal to 1 on the plasma/dielectric interfaces), respectively. Here, N_{total} and N_{charge} are the numbers of all species and charged species, respectively.

Usually, the LMEA and local field approximation (LFA) are commonly adopted in the numerical simulation of discharge plasma. The LFA shows simplicity and robustness [29]. In the near-wall region, where the plasma bottom side is close to the dielectric surface, the LFA may lead to an overestimation of ionization [26, 30]. And the LMEA shows more accuracy, especially in the positive streamer and plasma interacting with the dielectric [31]. To obtain more accurate data in the three-electrode pulsed SDBD, the LMEA is adopted in our numerical model. When the photoionization is considered in the numerical model, the streamer evolution can be described more accurately. The ionization of oxygen molecules by vacuum ultraviolet (VUV)-radiation comes from the electronically excited N_2 of the $\mathrm{b}^1\Pi_{\mathrm{u}}$, $\mathrm{b}'^1\Sigma_{\mathrm{u}}^+$ and $\mathrm{c}_4'^1\Sigma_{\mathrm{u}}^+$ states. The model is based on the assumption that the major contribution to the rate of photoionization comes from the radiation in the spectral range 98–102.5 nm; the radiation below 98 nm is absorbed by N_2, and the wavelength of 102.5 nm is the photoionization threshold of O_2. In addition, the three-exponential Helmholtz model [32, 33] has been implemented to calculate the photoionization source term S_{ph}

$$S_{\mathrm{ph}} = \sum_j S_{\mathrm{ph}}^j \tag{6}$$

$$\nabla^2 S_{\mathrm{ph}}^j - \left(\lambda_j p_{\mathrm{O}_2}\right)^2 S_{\mathrm{ph}}^j = -A_j p_{\mathrm{O}_2}^2 I \tag{7}$$

$$I = \xi \frac{p_{\mathrm{q}}}{p + p_{\mathrm{q}}} \alpha \mu E n_{\mathrm{e}} \tag{8}$$

Table 1. The kinetic reaction of air discharge in this numerical model.

No.	Reaction	Rate constant	References
R1	$e + N_2 \rightarrow N_2^+ + e + e$	$f(\sigma, \varepsilon_m)$	[35]
R2	$e + O_2 \rightarrow O_2^+ + e + e$	$f(\sigma, \varepsilon_m)$	[36]
R3	$e + O_2 \rightarrow O^- + O$	$f(\sigma, \varepsilon_m)$	[36]
R4	$e + N_2 \rightarrow e + N_2(C^3\Pi_u)$	$f(\sigma, \varepsilon_m)$	[35]
R5	$e + O_2 \rightarrow e + O + O$	$f(\sigma, \varepsilon_m)$	[36]
R6	$e + O_2 \rightarrow e + O + O(^1D)$	$f(\sigma, \varepsilon_m)$	[36]
R7	$e + N_2 \rightarrow e + N_2(A^3\Sigma_u)$	$f(\sigma, \varepsilon_m)$	[35]
R8	$e + N_2 \rightarrow e + N_2(B^3\Pi_g)$	$f(\sigma, \varepsilon_m)$	[35]
R9	$N_2^+ + N_2 + N_2 \rightarrow N_4^+ + N_2$	5×10^{-29}	[37]
R10	$N_2^+ + N_2 + O_2 \rightarrow N_4^+ + O_2$	5×10^{-29}	[37]
R11	$N_4^+ + O_2 \rightarrow O_2^+ + N_2 + N_2$	2.5×10^{-10}	[37]
R12	$N_2^+ + O_2 \rightarrow O_2^+ + N_2$	$6 \times 10^{-11}\ (300/T_{gas})^{0.5}$	[38]
R13	$O_2^+ + N_2 + N_2 \rightarrow O_2^+N_2 + N_2$	$9 \times 10^{-31}\ (300/T_{gas})^2$	[38]
R14	$O_2^+N_2 + N_2 \rightarrow O_2^+ + N_2 + N_2$	4.3×10^{-10}	[39]
R15	$O_2^+N_2 + O_2 \rightarrow O_4^+ + N_2$	1×10^{-9}	[39]
R16	$O_2^+ + O_2 + N_2 \rightarrow O_4^+ + N_2$	$2.4 \times 10^{-30}\ (300/T_{gas})^{3.2}$	[38]
R17	$O_2^+ + O_2 + O_2 \rightarrow O_4^+ + O_2$	$2.4 \times 10^{-30}\ (300/T_{gas})^{3.2}$	[38]
R18	$e + O_4^+ \rightarrow O + O + O_2$	$1.4 \times 10^{-6}\ (300/T_e)^{0.5}$	[37]
R19	$e + O_2^+ \rightarrow O + O$	$2 \times 10^{-7}\ (300/T_e)$	[37]
R20	$e + O_2 + O_2 \rightarrow O_2^- + O_2$	$2 \times 10^{-29}\ (300/\mathrm{T_e})$	[39]
R21	$O_2^- + O_4^+ \rightarrow O_2 + O_2 + O_2$	1×10^{-7}	[39]
R22	$O_2^- + O_4^+ + N_2 \rightarrow O_2 + O_2 + O_2 + N_2$	$2 \times 10^{-25}(300/T_{gas})^{3.2}$	[39]
R23	$O_2^- + O_4^+ + O_2 \rightarrow O_2 + O_2 + O_2 + O_2$	$2 \times 10^{-25}\ (300/T_{gas})^{3.2}$	[39]
R24	$O_2^- + O_2^+ + N_2 \rightarrow O_2 + O_2 + N_2$	$2 \times 10^{-25}\ (300/T_{gas})^{3.2}$	[39]
R25	$O_2^- + O_2^+ + O_2 \rightarrow O_2 + O_2 + O_2$	$2 \times 10^{-25}(300/T_{gas})^{3.2}$	[39]
R26	$O^- + N_2^+ \rightarrow O + N + N$	1×10^{-7}	[38]
R27	$e + N_4^+ \rightarrow N_2 + N_2(C^3\Pi_u)$	$2 \times 10^{-6}\ (300/T_e)^{0.5}$	[38]
R28	$e + N_2^+ \rightarrow N + N$	$2.8 \times 10^{-7}\ (300/T_e)^{0.5}$	[38]
R29	$N_2(C^3\Pi_u) \rightarrow N_2(B^3\Pi_g) + h\upsilon$	3.0×10^7	[38]
R30	$N_2(C^3\Pi_u) + N_2 \rightarrow N_2(B^3\Pi_g) + N_2$	0.13×10^{-10}	[37]
R31	$N_2(C^3\Pi_u) + O_2 \rightarrow N_2 + O + O(^1D)$	3×10^{-10}	[37]
R32	$N^+ + O_2 \rightarrow O_2^+ + N$	2.8×10^{-10}	[38]
R33	$O^+ + O_2 \rightarrow O_2^+ + O$	2×10^{-11}	[40]
R34	$O^- + O \rightarrow O_2 + e$	5×10^{-10}	[38]
R35	$O_2^- + O \rightarrow O_2 + O + e$	1.5×10^{-10}	[38]
R36	$N_2(A^3\Sigma_u) + O_2 \rightarrow N_2 + O + O$	$2.5 \times 10^{-12}\ (T_{gas}/300)^{0.5}$	[37]
R37	$N_2(B^3\Pi_g) + O_2 \rightarrow N_2 + O + O$	3×10^{-10}	[37]
R38	$N_2(B^3\Pi_g) + N_2 \rightarrow N_2(A^3\Sigma_u) + N_2$	1×10^{-11}	[37]
R39	$O(^1D) + O_2 \rightarrow O + O_2$	$3.3 \times 10^{-11}\ \exp(67/T_{gas})$	[37]
R40	$O(^1D) + N_2 \rightarrow O + N_2$	$1.8 \times 10^{-11}\ \exp(107/T_{gas})$	[37]

where λ_j and A_j indicate the fitting coefficients for the photoionization functions, which are obtained from [32]. Here, p_{O_2}, p_q and p are the partial pressure of O_2, the quenching pressure and ambient pressure, respectively; α and μE denote the Townsend ionization coefficient and the absolute drift velocity of electrons, respectively.

2.2.2. Reaction kinetic scheme. A suitable reaction kinetic scheme plays an important role in revealing the physical mechanism and the plasma evolution. There are a large number of species collision reactions in air discharge plasma. However, the numerical model coupled with whole reactions will significantly consume large computational time and many reactions are not important for the plasma behavior. As a result, a reduced kinetic reactions scheme, including the dominant ionization, excitation, attachment, charge transfer and recombination processes, is selected based on the corresponding pre-simulation and published works [34], as shown in table 1.

The rate constant unit of the three-body reaction is $cm^6{\cdot}s^{-1}$. The rate constant unit of the two-body reaction is $cm^3{\cdot}s^{-1}$. And the rate constant unit of the single-body reaction is s^{-1}. Here, T_{gas} and T_e indicate the gas temperature and electron temperature with the unit of K, respectively. The rate constants of the electron collision reaction (R1–R8) are calculated using BOLSIG+ [41].

2.2.3. Computational domain. To decrease the computational resources and time, a reduced computational domain

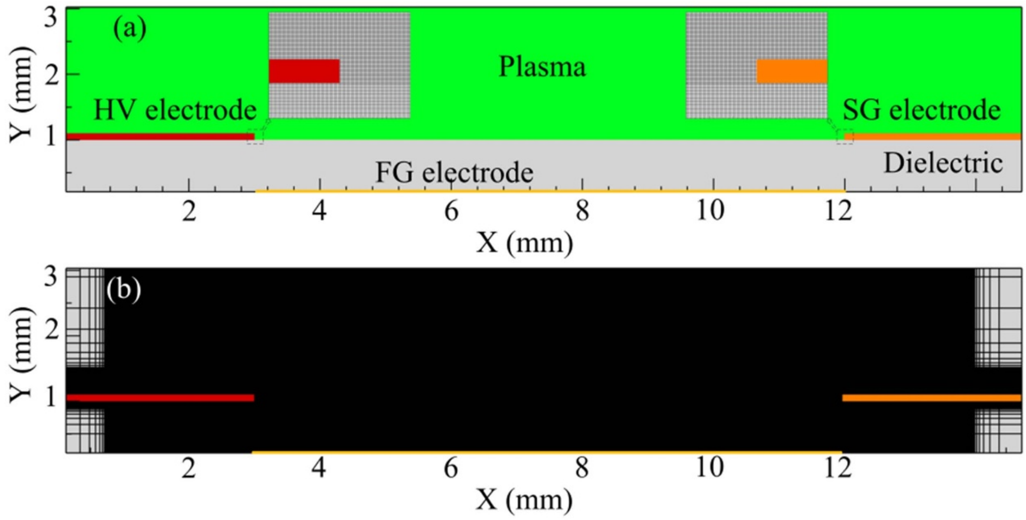

Figure 2. The numerical simulation geometry of (a) the calculated domain and (b) mesh.

with a dimension of $x \times y = 15$ mm $\times$ 3 mm is built based on the experimental configuration, as shown in figure 2(a). The widths of the HV electrode and SG electrode are set as 3 mm, and the thickness of both electrodes is set as 0.1 mm. The FG electrode is located at $y = 0$ with a length of 9 mm. Moreover, the dielectric is set as 1 mm thickness with a relative permittivity of 2.01. A structural mesh is utilized to discretize the computational domain. Due to the highly reduced electric field and species density in the vicinity of the metal electrode and dielectric surface, a uniform finer mesh of 6 μm $\times$ 6 μm is used for these domains. By considering the computational time and low species density variation in the other domain, a uniform coarse mesh of 15 μm $\times$ 15 μm is adopted for these domains (see figure 2(b)). Based on the above descriptions, 162 700 meshes are obtained for the three-electrode SDBD configuration of our physical model.

2.2.4. Initial and boundary conditions. The initial and boundary conditions also have significant requirements for the numerical calculation. For the initial conditions, the pressure is assumed to be 1 atm, which is similar to that of the experimental conditions. Two gas temperatures of 300 K and 500 K are set in the numerical model to analyze the effects of different gas temperature on the formation of discharge mode transition from surface-streamer to surface-spark discharge. Firstly, the gas temperature can be accumulated in the discharge region during the repetitive discharge [42]. Secondly, the primary streamer and transitional streamer also heat the gas, which can increase the gas temperature [43]. The steady-state temperature, at which every new streamer initiating the transient spark (TS) starts, is about ~550 K under high repetition frequencies of 10 kHz [43]. Considering the different experimental conditions of our work, a hypothetical gas temperature of 500 K is added into the model in a single pulse, which is utilized to reduce the computational burden of repetitive pulse discharge and analyze the effects of the gas temperature on the discharge mode transition. The initial electron density is set as $n_{e0} = 1 \times 10^{10}$ m^{-3}, which is uniformly distributed in the plasma domain. Furthermore, the ion density satisfies quasi-neutrality and the initial electron energy is 0.5 eV. For the Poisson's equation, the Dirichlet boundary condition is utilized for the metal surface. The non-metal boundary is set as Neumann boundary conditions. The applied pulse of the HV electrode comes from the oscilloscope recorded voltage data. And the FG electrode and SG electrode are set as grounded. During the three-pulsed SDBD, the produced charge can be deposited on the dielectric surface and the surface charge plays a critical role in the plasma behavior. In our numerical model, the surface charge is accumulated on the dielectric surface during each time step by collecting the charge flux flowing toward the dielectric on the boundary of the plasma region. The accumulated charge is stored in the edge of the finite volume mesh cell, and taken into account as additional charge when solving Poisson's equation. When the ions impact with the metal and dielectric surfaces, the secondary electron emission coefficient is assumed as 0.01.

2.3. 0D chemical kinetic modeling

It is a great challenge to produce a 2D plasma fluid simulation of a three-electrode SDBD driven by repetitive pulses, because the long inter-pulse period of two sequential pulses will consume a large computational cost. As a result, a 0D chemical kinetic model built in the ZDPlasKin [44] module incorporating BOLSIG+ [41] is developed to reduce the computational burden of the 2D plasma fluid model, which can be utilized to analyze the species evolution of the repetitive pulse discharge. Moreover, the Pumpkin code [45] is utilized to study the sensitivity coefficient of electron generation during different pulse discharge stages. There are 655 reactions, including 53 species of air discharge in the kinetic model. The reactions contain charged species, neutral species and excited species, including e, O^+, O_2^+, O_4^+, O^-, O_2^-, O_3^-, O_4^-, N^+, N_2^+, N_3^+, N_4^+, NO^+, N_2O^+, NO_2^+, $O_2^+N_2$, NO^-, NO_2^-, NO_3^-, N_2O^-, O_2, O, O_3, N_2, N, NO, N_2O,

NO_2, NO_3, N_2O_5, $O(^1D)$, $O(^1S)$, $O_2(4.5\ eV)$, $O_2(\upsilon = 1-4)$, $O_2(a^1\Delta_g)$, $O_2(b^1\Sigma_g^+)$, $N(^2D)$, $N(^2P)$, $N_2(\upsilon = 1-8)$, $N_2(A^3\Sigma_u^+)$, $N_2(B^3\Pi_g)$, $N_2(a'^1\Sigma_u^-)$ and $N_2(C^3\Pi_u)$. The cross-sections of electron collision reactions are selected from the Phelps database in LXCat [46]. Additionally, the reactions corresponding to the rate coefficients of plasma processes in nitrogen–oxygen mixtures are listed in these works [47, 48]. The reduced electric field is a significant input parameter in the 0D kinetic model and it can determine the discharge behavior, such as the species production and consumption. To enable the 0D kinetic model to have a better ability to describe the similar characteristics of the 2D numerical model, the temporal evolution of the reduced electric field for the 0D model is extracted from the fixed middle position ($x = 7.5$ mm and $y = 1.05$ mm) of the discharge channel in the 2D plasma fluid model. Also, the initial electron density is assumed to be $1 \times 10^{10}\ m^{-3}$, which is consistent with the 2D numerical model. Due to the intrinsic properties of the 0D model, it is difficult to describe the effect of electron losses on the wall surface, which should need the accurate rate coefficient of electron loss on the wall surface. However, the accurate rate coefficient is not easily obtained as it is affected by the different experimental conditions, including temperature and the dielectric material. Based on the electron drift–diffusion near the wall, it is found that the electron loss rate on the wall surface is far smaller than that of the space reaction. Moreover, the 0D kinetic model focuses on the species evolution driven by the sequential reduced electric field, which is utilized to describe the discharge behavior under repetitive pulse discharge. Therefore, the 0D mode neglects surface losses near the wall.

3. Results and discussion

3.1. Streamer evolution in three-electrode SDBD under repetitive pulses

The spatial-temporal evolution of discharge behavior involving electrical characteristics, optical diagnostics and streamer morphologies in the three-electrode pulsed SDBD driven by the original sequential five pulses under a 13 mm gap and 20 kV pulse voltage is illustrated in figure 3. It can be noted that every single pulse discharge consists of the primary, transitional and secondary reverse streamers in the five consecutive pulses. The three-electrode SDBD is developed from the traditional two-electrode SDBD, in which an SG electrode is arranged on the HV electrode side. Based on the SG electrode, a novel discharge phase, named as the transitional streamer, is formed and possesses varied properties compared to the two streamer phases in the two-electrode pulsed SDBD. According to the plasma morphologies with appearance time captured by the ICCD camera, three streamer phases characterized by different plasma behavior can be obtained in each pulse discharge. These three streamer phases can be distinguished through the appearance time. When the electric field around the HV electrode edge develops enough with the increasing pulse, the primary streamer ignites from the HV electrode and propagates along the dielectric surface. After the primary streamer reaches the SG electrode, some charges can be conducted from the SG electrode and the pulse voltage is still at a high value. Therefore, enough of an electric field strength is formed in the discharge gap, which can induce excitation and ionization processes. As a result, the transitional streamer is formed. Thereafter, the pulse voltage decreases to a value that is less than the electric potential formed by the accumulated charge. Then, a reversed electric field is generated from the HV electrode and dielectric surface. When the reversed electric field reaches a critical value of ionization and excitation processes, the secondary reverse streamer can be seen around the HV electrode. The detailed plasma behavior of three streamer phases in the individual pulse have been defined and investigated in our previous work [23]. For the transitional streamer, a similar discharge process can be obtained in the TS on pin-to-plate geometry, which has been studied in a series of works [49, 50]. Typically, the TS is initiated by a streamer and then transforms to a short spark phase. The streamer phase contains a primary streamer and a secondary streamer in the initial phase of the TS event [51]. When the primary streamer arrives at the cathode, the secondary is ignited from the anode and moves toward the cathode. After the secondary streamer bridges the discharge gap, a spark appears in a few more tens of nanoseconds. However, the primary streamer can almost instantly transition to the spark in the high-TS repetition frequency [52]. As a result, the streamer-to-spark transition should be a whole transitional process from streamer to spark in the TS discharge. It is not a single discharge process like the primary streamer or secondary streamer. Moreover, the streamer process is different from the TS discharge, which should be a primary streamer and transitional streamer in the three-electrode SDBD. Therefore, the transitional streamer may be more suitable for our work.

The three streamer phases show different plasma characteristics, including electrical and optical properties, in the sequential pulses. The positive current peak and optical emission intensity in the first pulse discharge are larger than those of subsequent pulses. This is because the memory effect [51, 53, 54] of residual positive charges produced by the previous pulse can reduce the electric field strength of subsequent applied pulses, which can furthermore inhibit the ionization and excitation processes. However, the negative current peak does not change significantly because it consists of an ion current, which is not sensitive to the electric field during the short timescale. Among the three streamer phases in the sequential pulses, the transitional streamer possesses more obvious differences than those of the primary and secondary reverse streamers. It can be seen that the transitional streamer is distributed uniformly in the discharge gap, because the residual surface charge generated by the primary streamer can induce a horizontal electric field and form a surface discharge. The plasma channel of the transitional streamer phase is concentrated in the domain of the HV electrode in the subsequent pulses. The reason for this can be attributed to the residual positive charges accumulating on the dielectric surface in the vicinity of the SG electrode, which will weaken the electric field in this domain. This phenomenon also results in the HV electrode region showing strong optical emission intensity in the subsequent pulse discharge.

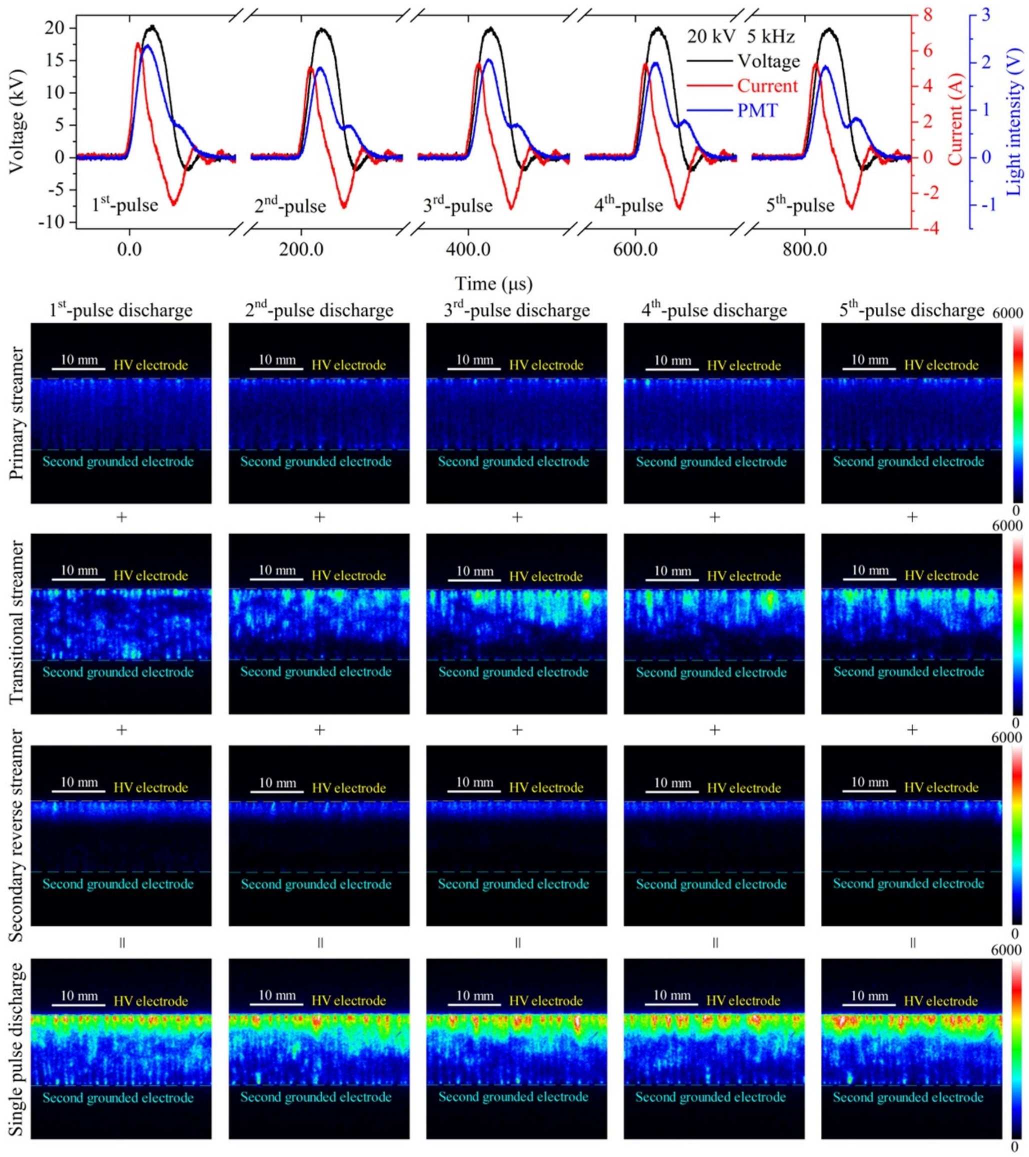

Figure 3. (Top) Voltage–current curves and optical emission intensity together with (bottom) the streamer morphology of three discharge phases in the original consecutive five pulses with 20 kV and 5 kHz under the discharge gap of 13 mm (the gain of the ICCD is set as 60 (the enhancement of light intensity)). The exposure time of the ICCD is varied with the duration of different discharge phases.

3.2. Discharge mode transition in sequential pulse

A surface-spark discharge can also be formed in the gap between the HV electrode and the SG electrode due to the lack of dielectric and the increasing reduced electric fields. Furthermore, the repetitive pulses can produce different discharge modes, which have been observed in [55, 56]. To obtain a deeper insight into the physical characteristics of the three-electrode SDBD driven by repetitive pulses, we investigate the main breakdown mechanisms that are responsible not only for the streamer dynamic evolution but also for the discharge mode transition under the discharge gap of 9 mm and pulse voltage of 19 kV. Two discharge modes of surface-streamer discharge, characterized by a low current, and surface-spark discharge, characterized by a high current, together with the corresponding waveforms of the voltage and current are measured, as demonstrated in figure 4. The surface-streamer discharge in a single pulse involves the primary and transitional streamers. The optical emission intensity of the secondary reverse streamer is not strong enough to be captured by the ICCD camera, because most accumulated charges are erased during the transitional streamer. Therefore, the reverse electric field decreases during the descending edge of the pulse voltage. Focusing on the second pulse under the pulse repetition frequency of 5 kHz, the secondary reverse streamer phase is replaced by a spark phase, which indicates that the pulsed surface-spark discharge consists of the primary streamer, the transitional streamer and the spark phase. After conductive plasma bridges are created in the discharge gap during the primary streamer, the transitional streamer appears, and then the transition from the transitional streamer to the spark phase is formed [57]. It can be indicated that the primary

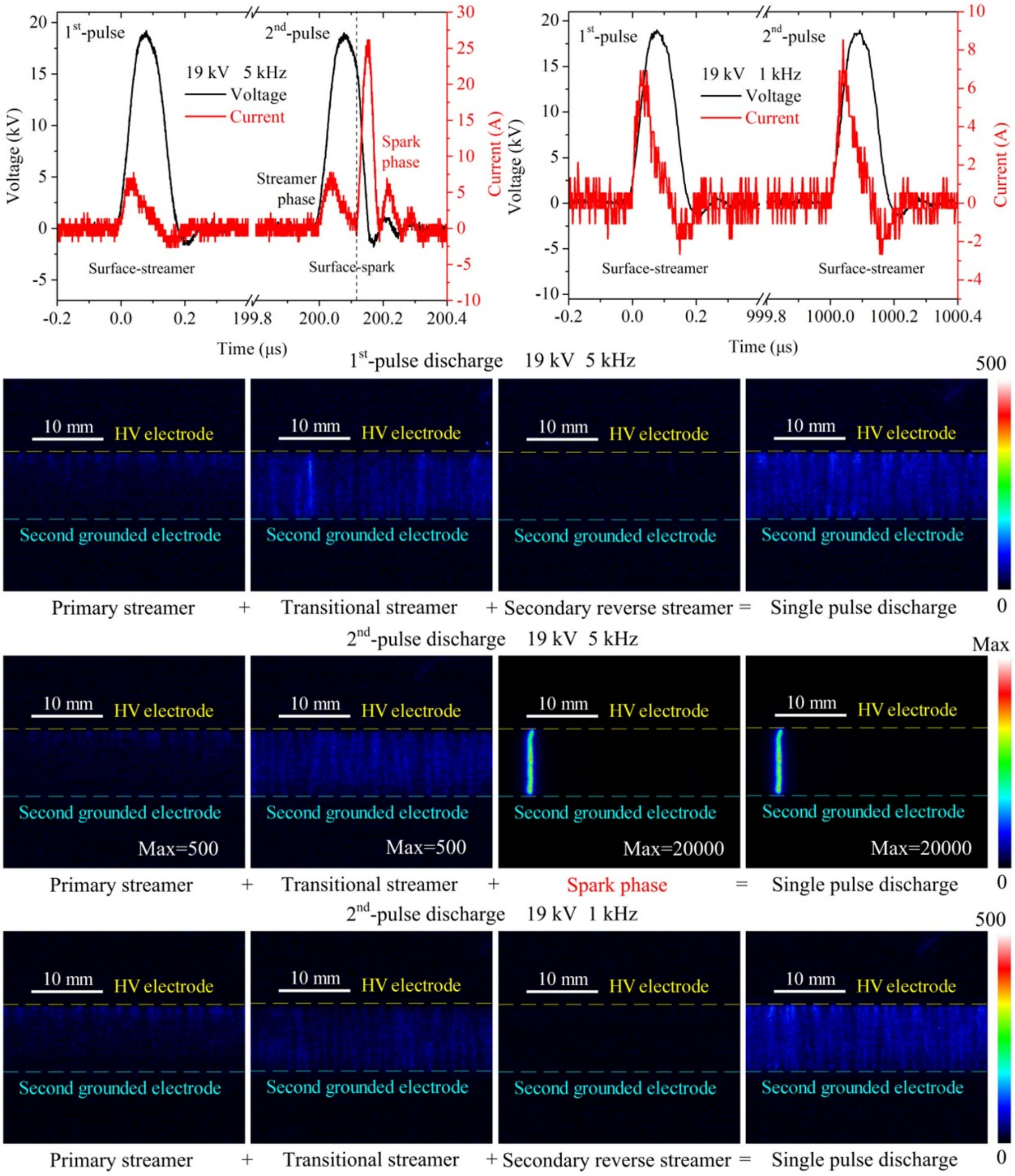

Figure 4. (Bottom) Two discharge modes of surface-streamer discharge and surface-spark discharge in a varied pulse repetition frequency together with (Top) the voltage and current waveforms under 19 kV and a discharge gap of 9 mm. (The gain of the ICCD is set as 1. The value of max for the color bar is varied with the light intensity of different discharge modes, as shown in the images.)

and transitional streamers play a significant role as it governs the preliminary process (the acceleration of detachment, stepwise and associative ionization) in the TS formation [49]. When the ionization rate in transitional streamer is improved, namely, the conductivity of the plasma channel increases enough, a spark discharge appears with a high current and a narrow plasma bridge is formed between the two electrodes at the same time [58]. In addition, a surface-streamer discharge, including the primary and transitional streamers, is still observed under the second pulse of 1 kHz repetition frequency. This is because more heat and active species are dissipated in the discharge domain during the large inter-pulse period, which contributes to the fact that the gas temperature cannot reach a critical value and the active species decrease to a low-density level.

3.3. Effect of the pulse repetition frequency on discharge mode transition

Based on the above descriptions, it is noted that the transition from surface-streamer discharge to surface-spark discharge can be obtained in the sequential pulses under the different pulse repetition frequencies. To analyze the effect of pulse repetition frequency on the discharge mode transition, the electrical characteristics of the pulse voltage and current under the different pulse repetition frequencies (1 kHz, 2.5 kHz and 5 kHz) are shown in figures 5(a)–(c). It can be seen that the pulsed surface-spark discharge can be observed in the sequential pulse and formed in the later pulse train of the low repetition frequency. This is due to the fact that the electrical energy injected into the gap through the streamer discharge

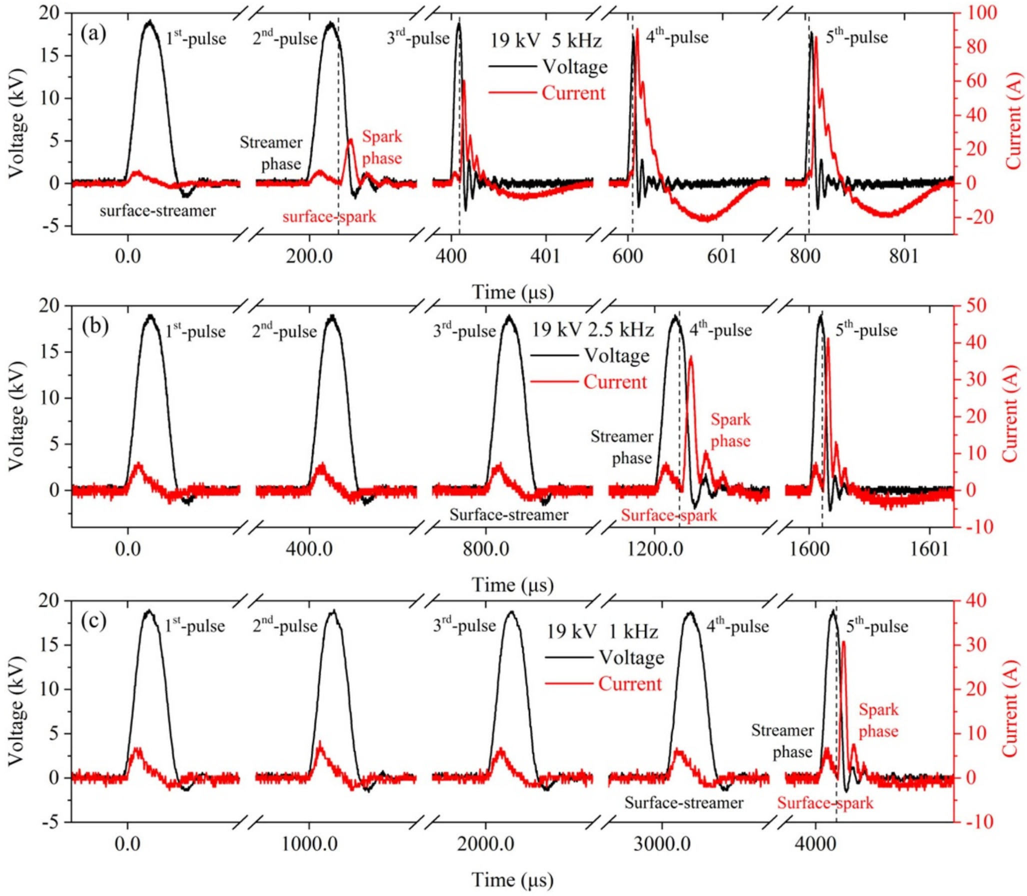

Figure 5. Typical pulse voltage and discharge current waveforms for the sequential pulses under three repetition frequencies of (a) 5 kHz, (b) 2.5 kHz and (c) 1 kHz.

can heat the gas and then results in the decrease in neutral molecule density, which will increase the reduced electric field [59]. However, the generated active species will stay in the discharge domain, which is beneficial to the electron production. Therefore, the transition from surface-streamer discharge to surface-spark discharge is formed. The heat accumulation and active species density need more time to reach the critical value for the formation of surface-spark discharge in the large decay time between voltage bursts; thus, the gas temperature rise and electron density increase need more pulse numbers under the low repetition frequency. In addition, the discharge current peak of the initial pulsed surface-spark discharge is lower than that in the subsequent pulse. This is because the previous pulsed surface-spark discharge can further raise the gas temperature, which can increase up to thousands of kelvin based on the thermal effect, thus enhancing the surface-spark discharge in the subsequent pulse [60, 61]. Also, more active species produced by the previous surface-spark discharge will promote the development of surface-spark discharge in the subsequent pulse. The detailed mechanism of streamer-to-spark transition will be analyzed in the following sections via the numerical simulation.

According to the measured voltage and discharge current, the mean discharge energy of sequential pulse discharge is obtained after three measurements, as shown in figure 6.

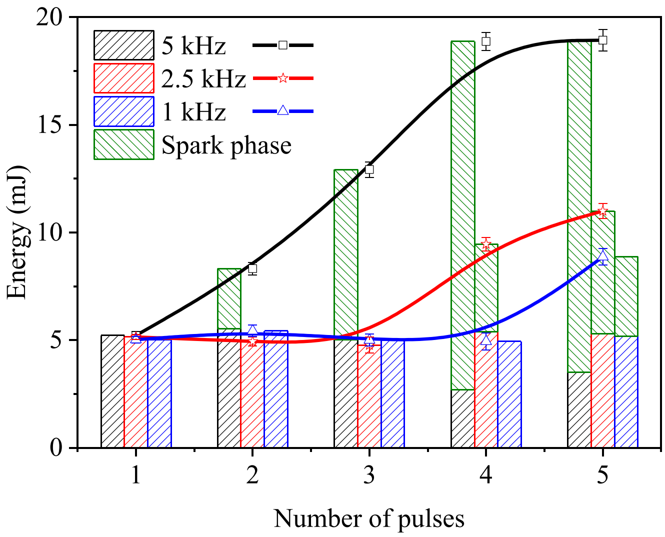

Figure 6. Electrical energy under different pulse repetition frequencies via experimental measurement.

The whole discharge energy increases with the occurrence of surface-spark discharge in sequential pulses due to its high discharge intensity. Furthermore, the discharge energy increases to a stable value when the surface-spark discharge

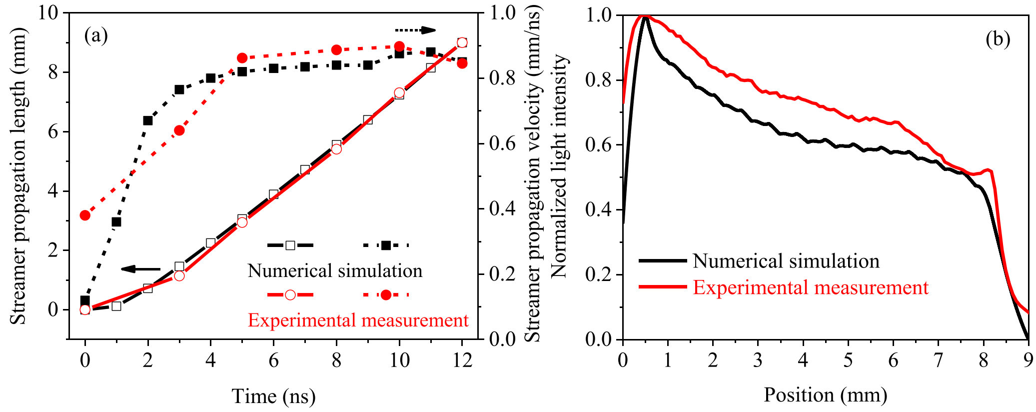

Figure 7. Comparison between numerical simulation and experimental measurement: (a) the primary streamer propagation position and velocity, and (b) the normalized luminous intensity of the whole pulse discharge.

reaches the steady state. The whole discharge energy increases from 5.22 mJ to 18.93 mJ under the pulse repetition frequency of 5 kHz. The discharge energy is 8.87 mJ in the fifth pulse under the pulse repetition frequency of 1 kHz, and the discharge energy is 11 mJ in the fifth pulse under the pulse repetition frequency of 2.5 kHz. For the surface-streamer discharge, the discharge energy remains basically unchanged, which is close to 5.1 mJ.

3.4. Numerical simulation by the 2D fluid model

Based on the descriptions of the above sections, the heat and active species play critical roles in the transformation of the surface-streamer discharge into surface-spark discharge in sequential pulses. To gain a deep insight into the mechanism of discharge mode transition in the three-electrode pulsed SDBD, a 2D plasma fluid model corresponding to the gas temperature of 300 K and 500 K is implemented. The validation of the developed 2D plasma fluid model is demonstrated via our experimental results, including plasma propagation characteristics, plasma morphology, discharge mode transition and discharge current. For the plasma propagation characteristics, the primary streamer propagation position and propagation velocity obtained by numerical simulation are compared with those of experimental measurements, as shown in figure 7(a). The streamer propagation position is measured by the ICCD camera with an exposure time of 5 ns and a different delay time. By changing the delay time of the ICCD, the primary streamer head position and propagation velocity will be obtained. From the results, it can be noted that the primary streamer propagation position and velocity of the numerical simulation are consistent with those of the experimental measurement. In the numerical simulation, the $N_2(C^3\Pi_u)$ density is usually utilized to indicate the luminous intensity due to the fact that the most streamer emission intensity comes from the $N_2(C^3\Pi_u)$ species [62]. Furthermore, the $N_2(C^3\Pi_u)$ density obtained by the numerical simulation agrees well with the streamer luminous intensity of the experimental measurement, as shown in figure 7(b). The maximal luminous intensity appears in the HV electrode region and then decreases along the primary streamer propagation.

For the plasma morphology and discharge mode transition, the electron density evolution in surface-streamer discharge and surface-spark discharge is shown in figures 8(a) and (b). From the results, it can be noted that the primary streamer is ignited from the edge of the HV electrode and propagates along the dielectric surface. When the primary streamer head is close to the SG electrode, a local discharge can be induced around the edge of the SG electrode. After the surface streamer bridges the HV electrode and SG electrode, the transitional streamer is sustained in the discharge gap. Furthermore, there are two discharge processes of the secondary reverse streamer and spark phase under the gas temperatures of 300 K and 500 K, respectively. This means that the surface-streamer discharge in the three-electrode pulsed SDBD is made of the primary, transitional and secondary reverse streamers. The surface-spark discharge in the three-electrode pulsed SDBD consists of the primary streamer, transitional streamer and spark phase. These numerical results are consistent with the experimental measurements in figures 3 and 4, which can prove the reliability of the developed 2D model. With regard to the formation of the spark phase, it is due to the fact that there are strong reduced electric field intensity and high electron density in the discharge gap after the transitional streamer under the high gas temperature [63]. When a large number of electrons are drifted by the electric field, the high ionization processes occur in the gap. As a result, the transitional streamer phase transforms into the spark phase.

The temporal evolution of the current, reduced electric field and electron density at the gas temperatures of 300 K and 500 K is presented in figures 9(a) and (b). The calculated current of the surface-streamer discharge agrees well with that of the experimental current, which can also demonstrate the validity of the numerical model. Compared to the results of the gas temperature at 300 K and 500 K, it is indicated that the streamer-to-spark transition happens at the maximal voltage value under a high gas temperature. At this time, the reduced electric field in the discharge gap is larger than that of the ionization threshold of air (120 Td) [62]. As a result, the electron density rises dramatically and then decreases when the applied electric field reduces. Meanwhile, the discharge current also increases to 33.3 A sharply and decreases with the descending

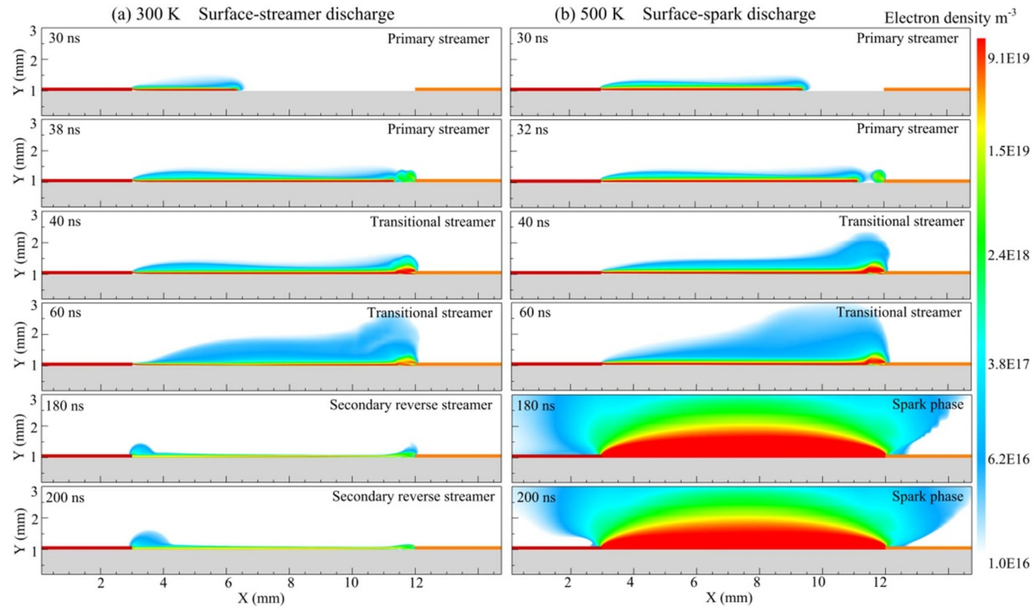

Figure 8. Evolution of electron density in the three-electrode pulsed SDBD under two gas temperatures: (a) surface-streamer discharge at 300 K, and (b) surface-spark discharge at 500 K.

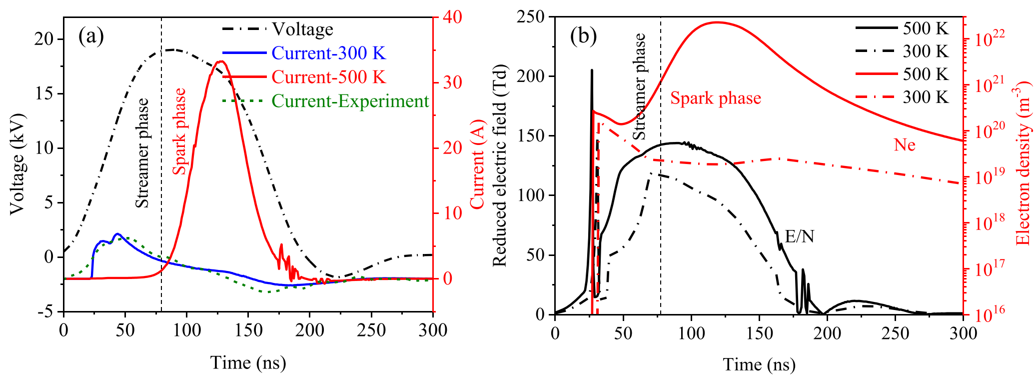

Figure 9. Temporal evolution of discharge dynamics in the three-electrode pulsed SDBD: (a) comparison of the calculated current and experimental current, and (b) temporal variations of the reduced electric field and electron density at the middle position of the discharge gap ($x = 7.5$ mm, $y = 1.05$ mm).

pulse voltage. It can also be seen that the electron density in the streamer phase does not have an obvious difference between the surface-streamer and surface-spark discharges. After the streamer phase, the electron density increases sharply under the effect of the spark phase with the strong ionization process, while it decreases because of the recombination process under a low reduced electric field.

The spatial distributions of electron density and reduced electric field at the line of $y = 1.05$ mm under the gas temperatures of 300 K and 500 K are analyzed in figure 10. During the streamer propagation phase (30 ns), a high reduced electric field with hundreds Td is formed in the streamer head [64], which has been reached hundreds Td. This is because a large number of positive charges have gathered in the streamer head and have induced a high-space electric field. However, a high electron density appears in the streamer channel due to the drift effect of the applied electric field. A high gas temperature results in a high electron density and large reduced electric field because of the strong excitation and ionization processes via the thermohydrodynamic mechanism [13]. After the streamer propagation phase (120 ns), the reduced electric field and electron density become more homogeneous along the discharge gap under the two gas temperatures. Furthermore, the electron density at the gas temperature of 500 K is larger than that at 300 K, which is caused by the fact that the reduced electric field becomes much larger than the ionization threshold of air (120 Td) along the discharge gap. The electron density reaches around 2.2×10^{22} m^{-3} under the gas temperature of 500 K, while it is around 1.9×10^{19} m^{-3} under the gas temperature of 300 K.

3.5. Electron evolution in repetitive pulses

The single pulse discharge with the effects of gas temperature has been analyzed via the 2D plasma fluid mode, as described in section 3.4. However, it is a large challenge for the 2D fluid

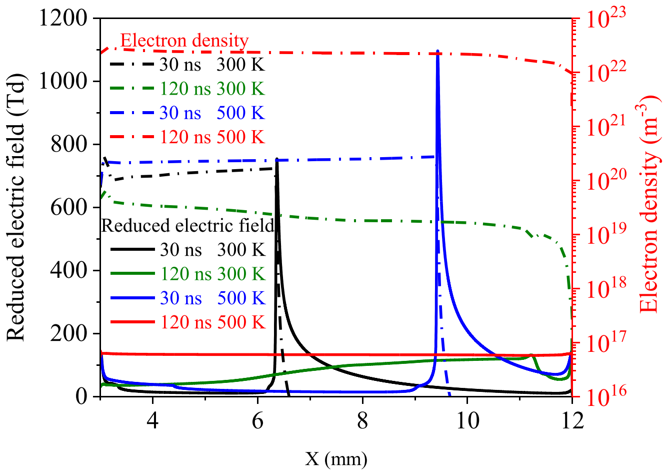

Figure 10. Spatial evolution of the electron density and reduced electric field at the line of $y = 1.05$ mm under the gas temperatures of 300 K and 500 K.

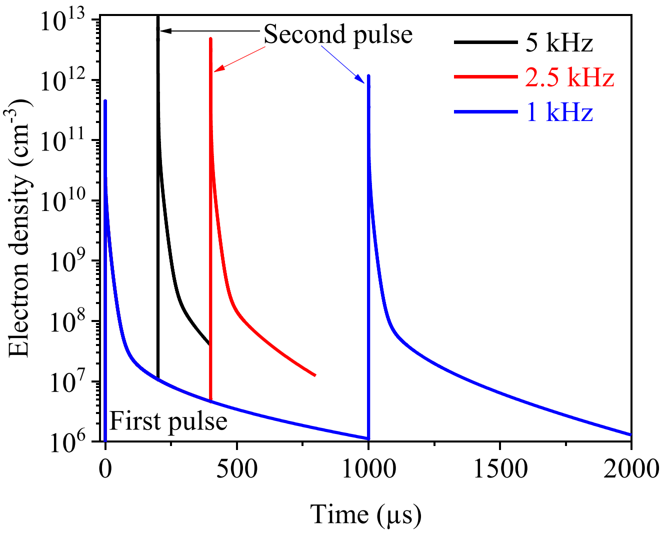

Figure 11. Temporal evolution of electron density for two sequential pulses with different pulse repetition frequencies under the gas temperature of 300 K.

model operated by sequential pulses due to the long computational time. As a result, a kinetic mechanism of repetitive pulses is implemented using the 0D numerical model under the gas temperature of 300 K, which has been described in section 2.3. The temporal evolution of electron density for the two sequential pulses with pulse repetition frequencies of 1 kHz, 2.5 kHz and 5 kHz is shown in figure 11. From the results, it is noted that the electron density increases with the applied reduced electric field during the pulsed discharge. After the discharge, the electron density decreases because of the recombination reactions under the low reduced electric field [65]. It can also be seen that the large-pulse repetition frequency will lead to a higher electron density during the second pulse discharge than that of the low-pulse repetition frequency. This is due to the fact that a short inter-pulse period will lead to high initial electron and excited species before the subsequent pulse, which is favorable for the production of electrons [66]. These results indicate that the species accumulation effect of the kinetic mechanism in a sequential pulse is beneficial to the re-ignition and ionization process of subsequent pulse discharge [13].

To gain further insight into the electron evolution through the repetitive pulses, the sensitivity coefficients of electron production for the first pulse discharge, the inter-pulse period and the second pulse discharge under the pulse frequency of 5 kHz and the gas temperature of 300 K are shown in figures 12(a)–(c). During the first pulse discharge phase, the electron is mainly generated by the N_2 and O_2 ionization reactions via the strong reduced electric field. And most electrons are consumed by the reaction of $e + O_2 \rightarrow O^- + O$. After the first pulse discharge, most electrons are consumed by the reactions of $e + O_2 + N_2 \rightarrow O_2^- + N_2$ and $e + O_4^+ \rightarrow O_2 + O_2$ during the inter-pulse period. Particularly, it is noted that most electrons are generated by the oxygen atom, including the reactions of $O_3^- + O \rightarrow O_2 + O_2 + e$ and $O_2^- + O \rightarrow O_3 + e$. This result indicates that the oxygen atom plays a critical role in electron generation during the inter-pulse period, thereby maintaining the electron density in the discharge gap after pulse discharge. The sensitivity coefficient of electron generation through the oxygen atom reaches 86%. The negative charges are generated through the recombination reactions, which means that the electron is stored in the negative charges. Then, the electron is released through the oxygen atom, which has also been reported by other studies [52, 62]. According to the electron release in the inter-pulse period via the kinetic mechanism, there is a high initial electron density for the subsequent pulse, which is beneficial for the ionization process. During the second pulse discharge, the production and consumption paths of most electrons are similar to those of the first pulse discharge. In addition, some electrons can be produced by $N_2(A^3\Sigma_u^+)$ and oxygen atom collision with negative charge, and some electrons will be consumed by O_4^+ and O_3.

3.6. Mechanism of surface-streamer transition into surface-spark

By combining the results of experimental measurements and numerical simulation, the formation mechanism of the transition from surface-streamer to surface-spark in sequential pulses can be obtained. For the formation of pulsed surface-spark discharge, a thermohydrodynamic mechanism and a kinetic mechanism are separately reported in some works [13, 49]. Thermohydrodynamics is based on the gas heating of a pulsed discharge, resulting in the gas temperature rising and the gas density decreasing. This phenomenon is beneficial for the increase of a reduced electric field and ionization rate. The kinetic mechanism corresponds to the accumulation effect of residual active species, which can modify the balance of electron generation and electron consumption through the acceleration of chemical reactions. It is also noted that the oxygen atom plays a dominant role in the formation of surface-spark discharge, which can release the electron from the negative

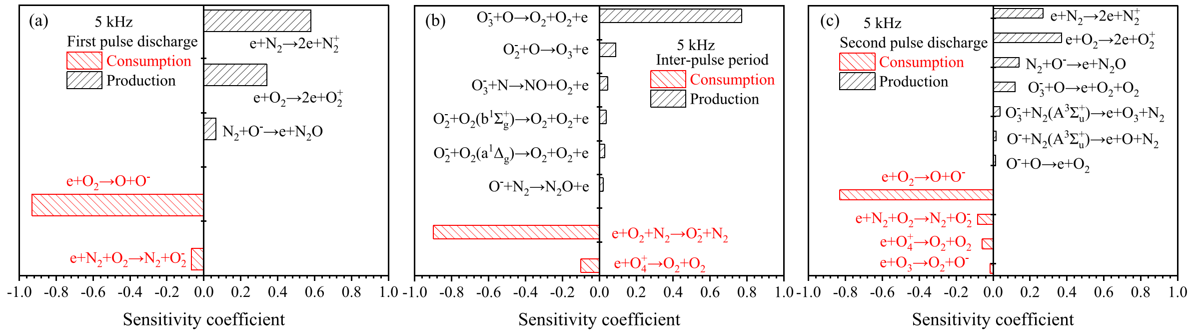

Figure 12. Sensitivity coefficients of electron production for dominant reactions under 5 kHz pulse frequency and 300 K gas temperature: (a) the first pulse discharge, (b) the inter-pulse period and (c) the second pulse discharge.

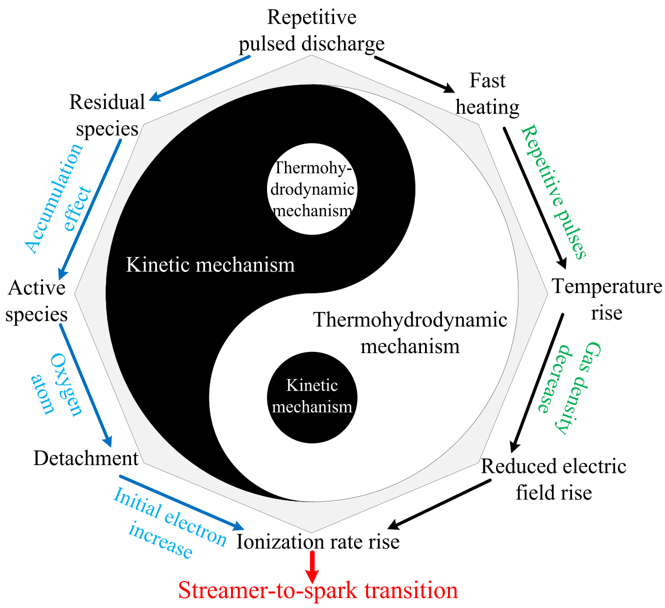

Figure 13. The mechanism for the formation of streamer-to-spark transition in a repetitive pulse.

charge through the collision reactions. Under the effects of repetition pulses, the two significant factors make contributions to the formation of pulsed surface-spark discharge inseparably, which is illustrated in figure 13. Firstly, the preceding surface-streamer discharges create a favorable environment for the formation of surface-spark discharge by developing a high gas temperature, which results in a highly reduced electric field and ionization rate. Secondly, the sequential discharge processes can provide memory effects of high densities for residual active species, and it can enhance the processes of detachment, stepwise and associative ionization, which are also beneficial for the increase of ionization rates [52, 67]. Also, the thermohydrodynamic mechanism and kinetic mechanism can promote and reinforce each other. Specifically, a high gas temperature is beneficial for the discharge, which can improve the active species density. And a high active species density will induce strong, fast gas heating, which can raise the gas temperature. As a result, the streamer-to-spark transition can be realized via these two effects in the repetitive pulses.

4. Conclusions

The streamer dynamic evolution and discharge mode transition in a three-electrode SDBD affected by repetitive pulses has been studied via experiments and numerical simulation. Because of the memory effect of residual charges produced by previous pulse discharge, the transitional streamer concentrates in the HV electrode domain and the plasma luminous intensity of the whole pulse discharge decreases in the subsequent pulses. When the ionization rate of the surface-streamer discharge is improved under the sequential pulses, a pulsed surface-spark discharge consisting of the primary streamer, transitional streamer and spark phase is formed in the gap. The discharge energy increases from 5.22 mJ, corresponding to a surface-streamer discharge, to 18.93 mJ of a surface-spark discharge under the pulse repetition frequency of 5 kHz. Upon decreasing the pulse repetition frequency, the pulsed surface-spark discharge will occur in a later pulse train because more heat and active species are dissipated during the large pulse-to-pulse intervals. A 2D plasma fluid model combined with a 0D chemical kinetic model is developed to analyze the effect of a thermohydrodynamic mechanism and a kinetic mechanism on contributing to the formation of streamer-to-spark transition in repetitive pulses. Upon comparing the numerical results of the gas temperature at 300 K and 500 K, a spark discharge is formed at the high gas temperature due to the fact that the reduced electric field exceeds the ionization threshold of 120 Td after the transitional streamer. At this time, the electron density reaches around 2.2×10^{22} m^{-3}. This also indicates that the active species play a critical role in the electron generation at the post discharge stage. Particularly, the oxygen atom can release the electrons from the negative charge of O_2^- and O_3^- with a sensitivity coefficient of 86% during the inter-pulse period. As a result, high initial electron density is maintained in the plasma region, which is favorable for the re-ignition and enhancement of subsequent pulse discharges.

Data availability statement

The data cannot be made publicly available upon publication because no suitable repository exists for hosting data in this field of study. The data that support the findings of this study are available upon reasonable request from the authors.

Acknowledgments

This work has been supported by the National Natural Science Foundation of China (Grant Nos. 52107140, 52177130 and 51877027). The authors gratefully acknowledge Dr Guanglin Yu (Dalian University of Technology), and Zhanqing Chen, Zhipeng Lei and Jiancheng Song (Taiyuan University of Technology) for their kind assistance and helpful discussions.

ORCID iDs

Bangfa Peng https://orcid.org/0000-0002-8690-0872
Nan Jiang https://orcid.org/0000-0003-4938-5864
Yifei Zhu https://orcid.org/0000-0001-8989-0051
Jie Li https://orcid.org/0000-0001-5557-8721

References

[1] Mursenkova I, Kuznetsov A Y and Sazonov A 2019 *Appl. Phys. Lett.* **115** 114102
[2] Rong M, Xia W, Wang X, Liu Z, Liu D, Liang Z, Zhang X and Kong M G 2017 *Appl. Phys. Lett.* **111** 074104
[3] Liu Y, Kolbakir C, Starikovskiy A, Miles R B and Hu H 2019 *Plasma Sources Sci. Technol.* **28** 014001
[4] Jiang N, Kong X, Lu X, Peng B, Liu Z, Li J, Shang K, Lu N and Wu Y 2022 *J. Clean. Prod.* **332** 129998
[5] Abdelaziz A A, Seto T, Abdel-Salam M, Ishijima T and Otani Y 2015 *J. Phys. D: Appl. Phys.* **48** 195201
[6] Ono R and Oda T 2006 *J. Phys. D: Appl. Phys.* **40** 176–82
[7] Peng B, He J, Liu Z, Yao X, Jiang N, Shang K, Lu N, Li J and Wu Y 2019 *J. Phys. D: Appl. Phys.* **52** 50LT01
[8] Lu X and Ostrikov K 2018 *Appl. Phys. Rev.* **5** 031102
[9] Kuthanová L and Hoder T 2022 *Plasma Sources Sci. Technol.* **31** 045022
[10] Brandenburg R 2017 *Plasma Sources Sci. Technol.* **26** 053001
[11] Li Y, van Veldhuizen E, Zhang G, Ebert U and Nijdam S 2018 *Plasma Sources Sci. Technol.* **27** 125003
[12] Nijdam S, Takahashi E, Markosyan A and Ebert U 2014 *Plasma Sources Sci. Technol.* **23** 025008
[13] Pancheshnyi S V, Lacoste D A, Bourdon A and Laux C O 2006 *IEEE Trans. Plasma Sci.* **34** 2478–87
[14] Zhao Z, Huang D, Wang Y, He J, Li C, Wang Y and Li J 2019 *Plasma Sources Sci. Technol.* **28** 085015
[15] Pai D Z, Lacoste D A and Laux C O 2010 *J. Appl. Phys.* **107** 093303
[16] Zhang Q-Z, Nguyen-Smith R T, Beckfeld F, Liu Y, Mussenbrock T, Awakowicz P and Schulze J 2021 *Plasma Sources Sci. Technol.* **30** 075017
[17] Zhang B and Zhang G 2017 *J. Appl. Phys.* **121** 105105
[18] Leonov S B, Adamovich I V and Soloviev V R 2016 *Plasma Sources Sci. Technol.* **25** 063001
[19] Hoder T, Synek P and Voráč J 2019 *Plasma Sources Sci. Technol.* **28** 105016
[20] Li T, Yan H-J, Li J-Q, Schulze J, Yu S-Q, Song J and Zhang Q-Z 2022 *Plasma Sources Sci. Technol.* **31** 055016
[21] Zhang Q-Z and Bogaerts A 2018 *Plasma Sources Sci. Technol.* **27** 105013
[22] Zhang Q-Z, Wang W-Z and Bogaerts A 2018 *Plasma Sources Sci. Technol.* **27** 065009
[23] Peng B, Shang K, Liu Z, Yao X, Liu S, Jiang N, Lu N, Li J and Wu Y 2020 *Plasma Sources Sci. Technol.* **29** 035018
[24] Peng B, Jiang N, Shang K, Lu N, Li J and Wu Y 2022 *J. Appl. Phys.* **55** 265202
[25] Zhu Y, Chen X, Wu Y and Starikovskaia S 2021 PASSKEy code (Science and Technology of Plasma Dynamics Laboratory; Laboratoire de Physique des Plasmas) (available at: www.plasma-tech.net/parser/passkey/)
[26] Zhu Y, Chen X, Wu Y, Hao J, Ma X, Lu P and Tardiveau P 2021 *Plasma Sources Sci. Technol.* **30** 075025
[27] Zhu Y, Shcherbanev S, Baron B and Starikovskaia S 2017 *Plasma Sources Sci. Technol.* **26** 125004
[28] Viehland L A and Mason E A 1995 *At. Data Nucl. Data Tables* **60** 37–95
[29] Bagheri B *et al* 2018 *Plasma Sources Sci. Technol.* **27** 095002
[30] Viegas P, Slikboer E, Bonaventura Z, Guaitella O, Sobota A and Bourdon A 2022 *Plasma Sources Sci. Technol.* **31** 053001
[31] Grubert G, Becker M and Loffhagen D 2009 *Phys. Rev.* E **80** 036405
[32] Bourdon A, Pasko V P, Liu N Y, Célestin S, Ségur P and Marode E 2007 *Plasma Sources Sci. Technol.* **16** 656–78
[33] Luque A, Ebert U, Montijn C and Hundsdorfer W 2007 *Appl. Phys. Lett.* **90** 081501
[34] Zhu Y and Starikovskaia S 2018 *Plasma Sources Sci. Technol.* **27** 124007
[35] Phelps A V and Pitchford L C 1985 *Phys. Rev.* A **31** 2932–49
[36] Lawton S A and Phelps A V 1978 *J. Chem. Phys.* **69** 1055–68
[37] Popov N 2011 *J. Phys. D: Appl. Phys.* **44** 285201
[38] Kossyi I, Kostinsky A Y, Matveyev A and Silakov V 1992 *Plasma Sources Sci. Technol.* **1** 207–20
[39] Pancheshnyi S, Nudnova M and Starikovskii A 2005 *Phys. Rev.* E **71** 016407
[40] Poggie J, Adamovich I, Bisek N and Nishihara M 2012 *Plasma Sources Sci. Technol.* **22** 015001
[41] Hagelaar G and Pitchford L 2005 *Plasma Sources Sci. Technol.* **14** 722–33
[42] Adams S, Miles J, Ombrello T, Brayfield R and Lefkowitz J 2019 *J. Phys. D: Appl. Phys.* **52** 355203
[43] Janda M, Machala Z, Niklová A and Martišovitš V 2012 *Plasma Sources Sci. Technol.* **21** 045006
[44] Pancheshnyi S, Eismann B, Hagelaar G and Pitchford L C 2008 Computer code ZDPlasKin (University of Toulouse, LAPLACE, CNRS-UPS-INP) (available at: www.zdplaskin.laplace.univ-tlse.fr)
[45] Markosyan A H, Luque A, Gordillo-Vázquez F J and Ebert U 2014 *Comput. Phys. Commun.* **185** 2697–702
[46] Phelps database plasma data exchange project (available at: https://www.lxcat.net/Phelps) (Accessed 3 August 2021)
[47] Capitelli M, Ferreira C M, Gordiets B F and Osipov A I 2000 *Plasma Kinetics in Atmospheric Gases* vol 31 (Springer Science & Business Media)
[48] Flitti A and Pancheshnyi S 2009 *Eur. Phys. J. Appl. Phys.* **45** 21001
[49] Naidis G 1999 *J. Phys. D: Appl. Phys.* **32** 2649–54
[50] Janda M, Martišovitš V, Hensel K, Dvonč L and Machala Z 2014 *Plasma Sources Sci. Technol.* **23** 065016
[51] Janda M, Hoder T, Sarani A, Brandenburg R and Machala Z 2017 *Plasma Sources Sci. Technol.* **26** 055010
[52] Janda M, Martišovitš V, Buček A, Hensel K, Molnár M and Machala Z 2017 *J. Phys. D: Appl. Phys.* **50** 425207

[53] Pietanza L, Colonna G, Laricchiuta A and Capitelli M 2018 *Plasma Sources Sci. Technol.* **27** 095003
[54] Li T, Yan H-J, Yu S-Q, Wang Y-Y, Li J-Q, Song J and Zhang Q-Z 2022 *J. Appl. Phys.* **132** 153301
[55] Zhao Z, Li C, Zheng X, Sun A and Li J 2022 *Plasma Sources Sci. Technol.* **31** 045005
[56] Pai D Z, Stancu G D, Lacoste D A and Laux C O 2009 *Plasma Sources Sci. Technol.* **18** 045030
[57] Wang D and Namihira T 2020 *Plasma Sources Sci. Technol.* **29** 023001
[58] Cernak M, Hoder T and Bonaventura Z 2020 *Plasma Sources Sci. Technol.* **29** 013001
[59] Tholin F and Bourdon A 2014 *Plasma Phys. Control. Fusion* **57** 014016
[60] Pai D Z, Lacoste D A and Laux C O 2010 *Plasma Sources Sci. Technol.* **19** 065015
[61] Lo A, Cessou A, Lacour C, Lecordier B, Boubert P, Xu D, Laux C and Vervisch P 2017 *Plasma Sources Sci. Technol.* **26** 045012
[62] Chen X, Zhu Y and Wu Y 2020 *Plasma Sources Sci. Technol.* **29** 095006
[63] Tholin F and Bourdon A 2013 *J. Phys. D: Appl. Phys.* **46** 365205
[64] Jánský J, Bessiéres D, Brandenburg R, Paillol J and Hoder T 2021 *Plasma Sources Sci. Technol.* **30** 105008
[65] Orrière T, Moreau E and Pai D Z 2018 *J. Phys. D: Appl. Phys.* **51** 494002
[66] Tyl C, Lin X, Bouzidi M C, Dap S, Caquineau H, Ségur P, Gherardi N and Naudé N 2018 *J. Phys. D: Appl. Phys.* **51** 354001
[67] Janda M, Machala Z, Dvonč L, Lacoste D and Laux C O 2014 *J. Phys. D: Appl. Phys.* **48** 035201